Renewable and Sustainable Energy Reviews 97 (2018) 497–508

Contents lists available at ScienceDirect

Renewable and Sustainable Energy Reviews

journal homepage: www.elsevier.com/locate/rser

Vulnerability of European intermittent renewable energy supply to climate change and climate variability

P. Ravestein[a], G. van der Schrier[b], R. Haarsma[b], R. Scheele[b], M. van den Broek[a,*]

[a] Copernicus Institute of Sustainable Development, Utrecht University, Utrecht, the Netherlands
[b] Royal Netherlands Meteorological Institute (KNMI), the Netherlands

ARTICLE INFO

Keywords:
Climate simulations
North Atlantic Oscillation
Climate
Change
Intermittent renewable energy sources

ABSTRACT

The impact of both climate change and climate variability on the supply of intermittent renewable energy sources (I-RES) in Europe are assessed based on global climate model simulations. The main driver of climate variability over Europe is the North Atlantic Oscillation (NAO) in winter and its equivalent in summer (sNAO) which determine to a large extent the atmospheric circulation in Europe. Four climate scenarios are constructed distinguished by a moderate and strong increase of the average global surface temperature, and a positive and negative phase of the atmospheric variability over the North Atlantic and Europe. This spans a framework which combines the effects of both climate change and climate variability. Using a 2050 distribution of PV panels and wind turbines, we found that although climate change is likely to have significant impact on future I-RES output in Europe, its effects, especially for wind power, are outweighed by the high and strongly variable impact of the NAO/sNAO phases. Variability in the large-scale atmospheric circulation is able to induce median I-RES yield differences of 20–30% for high wind potential regions. Due to the NAO variability also months were identified with persistent calm conditions over Europe linked to the inflow of frigid arctic air resulting in some regions in a decrease in wind power of up to 75%a accompanied with an increase in heating degree days of up to 30%. The results of the study imply that if requirements for the power system including back up capacity take into account the weather variability, the power system can also cope with the climate change impacts.

1. Introduction

Intermittent renewable energy sources (I-RES), such as wind and solar power, need to contribute significantly to the reduction of greenhouse gas emissions [1]. However, the dependency of I-RES on local weather conditions renders power output from I-RES vulnerable to climate change and natural climate variability. Earlier studies [2–6] investigating the relation between climate change and I-RES, found a relatively small impact of climate change on wind and solar power generation, with regional differences in these trends over Europe. Using the latest EURO-CORDEX regional climate models in combination with newly developed capacity scenarios [7–10], a small decrease was found in annual wind power for southern Europe with more stable wind power production in northern Europe [10] in combination with a decrease in irradiation in northern Europe and an increase in southern Europe [8].

Natural climate variability is caused by variations in large-scale atmospheric circulation patterns which strongly modulate the temperature, wind, and irradiation for large parts of Europe. The North Atlantic Oscillation (NAO) is the most important mode of atmospheric variability over the North Atlantic sector in the winter, and plays a major role in weather and climate variation over eastern North America, the North Atlantic, and the Eurasian continent [11]. The NAO can be in a positive or a negative phase, relating to the sign of the NAO index, which is the normalized atmospheric pressure differences between the Azores and Iceland (and is one way of quantifying the variations in pressure difference between the subtropics and the subpolar regions). When the pressure difference in the NAO is higher or lower than average, it is in its positive or negative phase, respectively. In the winter, a positive NAO generally leads to windy conditions in northern Europe, with a south-westerly wind bringing mild, cloudy and rainy weather, while southern Europe enjoys relatively sunny and dry conditions. With a negative NAO, the storm track over the North Atlantic ocean is located much more to the south, bringing cloudy and windy conditions to the southern part of Europe while northern Europe generally has calm, cool and dry weather [12]. The equivalent of NAO in the summer season, the so-called summer North Atlantic Oscillation (sNAO), is characterised by a more northerly location of the high- and low-pressure areas over the North Atlantic and a smaller spatial scale than its winter counterpart [13]. While the sNAO is the dominant mode

* Corresponding author.

https://doi.org/10.1016/j.rser.2018.08.057
Received 20 October 2017; Received in revised form 29 August 2018; Accepted 29 August 2018

of atmospheric variability in the summer, it explains less the prevailing weather patterns than the NAO.

Note that the NAO is only one mode of atmospheric variability and many systems are in use to characterize the variability of the atmosphere of the North Atlantic/European sector in terms of recurring patterns. An overview of these patterns for Europe and their impact on temperature is provided by e.g. [14].

A strong relation is found between the NAO phases and I-RES output. Brayshaw et al. [15] further analysed this relation and concluded that the NAO has a significant impact on the hourly-, daily- and monthly-mean power output distributions of the turbines in wind farms. For the Iberian Peninsula the negative NAO phase enhances the wind speed (10–20%) and reduces the irradiation (10–20%) [16]. Results with similar magnitudes were found for northern regions in Europe [17] while for the Mediterranean region year-to-year variations of over 20% in winter I-RES output was found [18]. While the climate change effect on I-RES output is relevant, the impact of natural climate variability like the (s)NAO, is shown to have a strong impact on I-RES as well, in combination with the observation that the (s)NAO is variable and difficult – if not impossible – to predict. This points to the necessity of considering climate change and climate variability in combination rather than as separate drivers of I-RES trends and variations. Insights into the combined impact on I-RES can guide policy makers, transmission system operators, distribution system operators, and electricity producers, with designing their strategies (e.g. investments in generation, storage and backup capacity, and interconnections). The aim of this study is, therefore, to provide such a combined evaluation of the impact of future weather on I-RES output. This study focusses on Western Europe and evaluates the impacts for the year 2050. For this purpose, historical weather data from observations and future weather data from a climate model with high spatial resolutions are combined with distributions of onshore and offshore wind turbines and photovoltaic systems (PV). Other sources of I-RES, like hydropower, are not considered. Furthermore, possible negative effects of climate change such as icing, corrosion, and abrasion due to airborne particles, are neglected. Finally, this research is limited to analysis of I-RES output in the winter and summer, as in these seasons the dominant modes of climate variability are well-defined in the (s)NAO processes.

2. Methods

With the climate model, EC-Earth (Section 2.1) four scenarios of future weather data were created to span the spectra of climate change and climate variability (Section 2.2). Next, the results of these four scenarios were combined with spatial distributions of I-RES (Section 2.3) to calculate the I-RES generation across Europe (Section 2.4). Finally, the resulting generation profiles were compared with generation profiles based on observational weather data.

2.1. Climate model

The climate model used is the EC-Earth model [19] which is a state-of-the-art global coupled earth system model, consisting of the Integrated Forecast System (IFS) of the European Centre for Medium Range Weather Forecasts (ECMWF) as the atmosphere component and the Nucleus for European Modelling of the Ocean (NEMO) developed by Institute Pierre Simon Laplace (IPSL) as the ocean component. We use EC-Earth version 2.3 employing IFS cycle 31R1, which has been modified in order to meet the requirements for climate research. For our study we use a horizontal spectral resolution of T159 in the dynamical core of IFS and a corresponding N80 reduced Gaussian grid (~1.125° × 1.125°) for the computation of physical processes. In the vertical there are 62 hybrid model levels extending up to about 5 h Pa (~37 km). The time stepping is done using a semi-Lagrangian advection scheme, permitting a time step as large as 1 h in T159. The EC-Earth model has shown to successfully model large scale circulation above the Atlantic and Europe [19] and compares to the median of the CMIP5 suite of climate models.

2.2. Climate scenarios and data sets

With EC-Earth an ensemble of 16 simulations for the period 1950–2100 is made assuming a RCP 8.5 emission pathway. Each simulation is initialized differently, aiming to span the full spectrum of internal climate variability and provides an equally probable and realistic estimate of day-to-day weather consistent with the emission pathway.

The ensemble was divided into four scenarios based on two parameters: global temperature, and atmospheric circulation, represented by the (s)NAO index. Since the relation between global temperature and greenhouse gas is well-understood and linear, data from the 2051 to 2065 period are taken to represent climatic conditions with a strong global warming while data from the 2036–2050 period represent climatic conditions with a moderate warming. The impact of atmospheric variability is captured by labelling each winter and summer season by the phase of the NAO and sNAO, respectively. This division in moderate (M) and high (H) warming and positive (≥ 0) and negative (<0) (s)NAO index resulted in the four scenarios: M+, M-, H+ and H-, where e.g. M + represents a moderate global warming with a dominantly positive (s) NAO index.

The terminology to refer to 'M' and 'H' scenario's relates to approach of the climate scenario's issued by the Royal Netherlands Meteorological Institute [20]. The principal reason for using this terminology is that the KNMI'14 scenario's are defined for two time horizons: 2050 and 2085. For the moderate (M) scenario's, the 2050 time horizon corresponds to a global mean temperature increase of 1 °C (and 1.5 °C for 2085). The high (H) scenario's relate to a global mean temperature increase of 2 °C in 2050 (and 3.5 °C in 2085). These values are relative to the 1981–2010 climatic mean.

The 16 simulations of the EC-Earth climate simulations thus resulted in approximately 120 winter and 120 summer variants per scenario (15 years times 16 simulations of which about half with a positive and the other with a negative (s)NAO index). The 480 variants can be considered as many different projections of potential weather in 2050 and are not long time series of successive years. The relevant output parameters of the EC-Earth climate model for this research are presented in Table 1.

The General Circulation Models (GCMs) that provide climate simulations usually suffer from biases in their output. This bias needs correction. The standard procedure to quantify the biases by comparing the model climatology for the current climate with that of observations. In this study, the model climatology is simply adjusted by subtracting this bias. The motivation of this approach is that a climate model may

Table 1
Types of output of the EC-Earth model relevant for this research.

Type of data	Unit
Daily average Radiation Surface Downward Short wave (RSDS) (includes direct and diffuse irradiation)	W/m^2
Daily average wind speed at 10 m height (AWS)	m/s
6 hourly wind speed at 80 m height (V)	m/s
6 hourly wind speed at 100 m height (V)	m/s
6 hourly wind speed at 120 m height (V)	m/s
6 hourly wind speed at 150 m height (V)	m/s
Average daily temperature at 2 m height (T_{AVG})	°C
Daily maximum temperature at 2 m height (T_{MAX})	°C

Table 2
Wind and PV capacity per region for the ECF 80% renewables pathway in 2050 in GW [24].

In GW	Wind onshore	Wind offshore	PV
Nordic (Denmark, Norway, Sweden, Finland)	37.5	38.5	23.0
United Kingdom and Ireland	49.0	57.0	46.0
Benelux and Germany (The Netherlands, Belgium, Luxemburg, Germany)	32.0	67.0	114.0
Iberian Peninsula (Spain, Portugal)	43.0		180.0
France	32.0	19.0	133.0
Poland and Baltic (Poland, Estonia, Latvia, Lithuania)	10.5	10.5	50.0
Central Europe (Austria, Czech Republic, Slovakia, Slovenia, Switzerland)	16.0		137.0
South-East Europe (Bulgaria, Cyprus, Greece, Hungary, Romania)	5.0		76.0
Italy and Malta	22.0		121.0
Total	247.0	192.0	880.0

have a bias in representing the current state of the climate, it will be reliable in simulating the *change* in climate. Appendix A provides more detail on the bias correction.

The EC-Earth simulations were corrected by comparing them to 30 years of observational data (1981–2010) from three different sources. The E-OBS dataset provided the observed temperature data [21], and the HIRLAM reanalysis dataset from the EU-project EURO4M provided the observed irradiation and wind speed at 10 m height data [22]. These reanalysis datasets were regridded to match the 0.25° x 0.25° latitude-longitude grid of the E-OBS dataset. Finally, the ERA Interim [23] dataset was used for high altitude wind speed data as these were unavailable in the E-OBS and HIRLAM reanalysis datasets. Furthermore, the EC-Earth outputs were regridded to a regular 0.25° × 0.25° grid before the model's biases could be corrected (see Appendix A for further details).

2.3. Geographical distribution of future installed I-RES capacity over Europe

To assess the I-RES output across Europe, this study used spatial distributions of PV and wind turbines created with the CLIMIX model [7]. These distributions were developed earlier for PV [8] and wind [9] and are based on capacities per European region (see Table 2) from the 80% renewable pathway by the ECF [24]. The capacities were distributed over each region's grid cells based on wind and solar resource quality, population density, and land cover.

The capacity distributions for both PV and wind turbines are shown in Fig. 1. The starting points of these distributions were the locations of the already installed PV and wind capacity in 2012. The CLIMIX model then spatially distributed new solar and wind capacity based on full load hours potential, population and land use in the different regions in accordance with the ECF 80% renewable pathway. It was assumed that all new turbines have a hub height of 100 m onshore, and 150 m offshore.

Alternative future capacity distributions for Europe than the ones used in this study based on the CLIMIX study [7] are those by Schlachtberger et al. [25]. They set their geographic installation potential of PV, onshore and offshore wind in each country proportional to the usable area and potential full load hours until a threshold is reached. For both onshore and offshore wind power, a combination of restrictions in the availability of areas and public acceptance issues led to a threshold of 2 MW/km^2. The threshold for PV is based on a limit of 1% of the area that can be used for solar PV panels with a nominal capacity of 145 MW/km^2. Next, their geographical capacity distributions were determined by minimizing investment costs of generation technologies and transmission lines. The resulting alternative capacity distributions affect the estimates of renewable energy generated, but the variation between the four scenarios used in this study are believed to be robust for these variations in assumptions on the installed capacity.

2.4. Power production

The conversion from irradiation and wind speed data to electricity

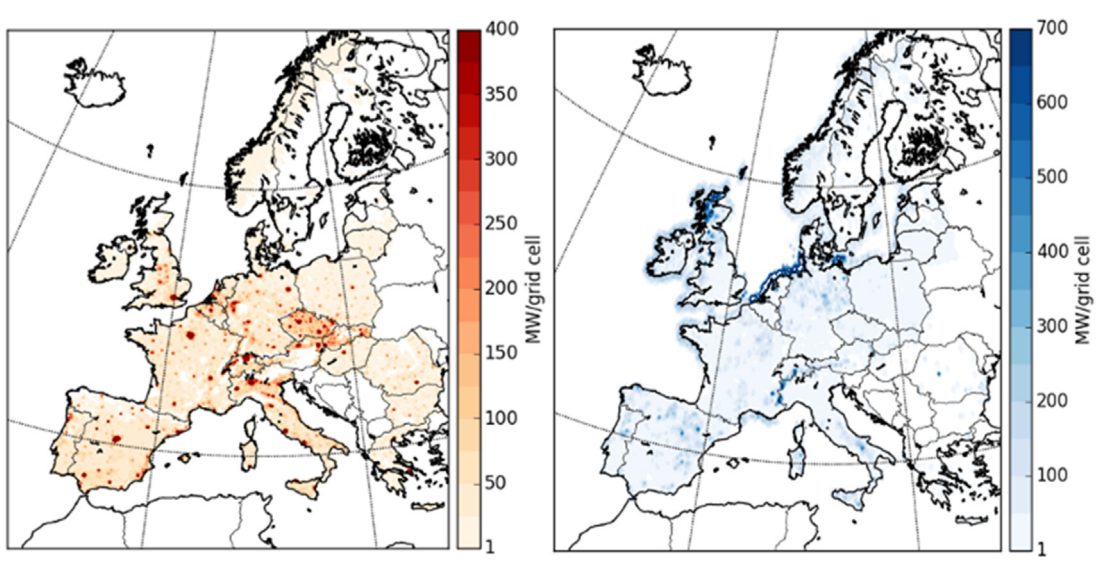

Fig. 1. Distribution of 880 GW PV (left) and 440 GW wind turbines (right) over Europe in 2050, produced with the CLIMIX model with a spatial resolution of 0.11° latitude-longitude (figure based on data from [7,8,10]).

generation is performed with the same methods as Jerez et al. [8,16] and Tobin et al. [9,10]. The calculation of I-RES electricity output in a grid cell depends on two factors: the I-RES potential per timestep and grid cell and the installed capacity per grid cell. See Eq. (1) for wind and Eq. (2) for PV.

$$PO_{h,g} = Wpot_{h,g} \times IC_g \times SEC_h \tag{1}$$

$$PO_{d,g} = PVpot_{d,g} \times IC_g \times SEC_d \tag{2}$$

where $PO_{h,g}$ (MJ) is the electricity output per grid cell and timestep (daily or 6-hourly), $Wpot_{h,g}$ and $PVpot_{d,g}$ the wind and PV potentials per grid cell and timestep, IC_g (MW) the installed capacity per grid cell, and SEC the number of seconds in the daily or 6-hourly timestep. The subscripts g, h, and d are indices for the sets of grid cells, 6-hourly timesteps, and daily timesteps, respectively.

PVpot and Wpot can be seen as capacity factors indicating at which percentage of the nominal capacities PVs or wind turbines operate under the weather conditions in a specific grid cell and timestep [16]. PVpot is derived from the daily RSDS outputs of the EC-Earth model and the length of these days are based on the average amount of hours with irradiation per season for De Bilt in 2014 (8.8 in the winter, 16 in the summer). Wpot is based on 6 hourly wind speed data from EC-Earth and therefore calculated with 6 hourly timesteps.

The diurnal cycle in wind is strong and the relation to wind potential strongly non-linear, which motivates to use a timestep in the wind data which is as short as possible, and the wind data from EC-Earth are outputted at 6-hourly resolution. The 6-hourly wind potential is subsequently aggregated to the daily level. For the PV potential, the relation between solar radiation and PV is close to linear, which allows for using a daily sum of radiation.

Note that a realistic representation of complex topography or land-sea contrasts require a spatial detail in the climate simulations which is not provided by the EC-Earth simulations. This affects the estimates of the Wpot and PV. However, as all four scenario's are affected equally, the findings of this study are not affected by this.

2.4.1. PV power production calculation

PVpot is based on a comparison between specific weather conditions (irradiation, daylight temperature, wind speed) and weather conditions under Standard Test Conditions (STC) [26]:

$$PVpot_{d,g} = PR_{d,g} \times \frac{RSDS_{d,g}}{RSDSstc_d} \tag{3}$$

Where RSDS is the average surface downward short wave radiation (wave length 0.2–0.4 μm) (W/m^2), RSDSstc is the RSDS under standard test conditions, 1000 (W/ m^2), and PR the performance ratio. The performance ratio incorporates the deviation from the STC in a real life situation [26] and is around 85% for modern PV modules [27]. This is corrected for actual temperature development:

$$PR_{d,g} = 0.85 + Y\,(T_{d,g} - Tstc) \tag{4}$$

Where T is the PV module temperature (°C), Y is the response of typical monocrystalline silicon solar panels of 0.41% /°C, and Tstc is the temperature under standard test conditions (25 °C) [28].

The PV module temperature is modelled considering the effects of the daylight temperature (TAS), irradiation (RSDS), and wind speed (VWS) [28]:

$$T_{d,g} = 0.943TDL_{d,g} + 0.028RSDS_{d,g} - 1.528AWS_{d,g} + 4.3 \tag{5}$$

Where AWS is the average wind speed at 10 m height (m/s), TDL is the estimated temperature during daylight [(Tavg +Tmax) / 2] (°C), and Tmax the daily maximum temperature.

2.4.2. Wind power production calculation

Wpot is based on wind speed in combination with an average power curve. Power curves tend to overestimate the produced electricity compared to measured turbine production. However, they are an easy and effective method of estimating a wind turbine's power production, and are used inter alia for pre-construction financial analysis, and to measure subsequent operational efficiency [29].

A turbines power curve contains three characteristic wind speed values: the cut-in speed, rated speed, and cut-out speed. The cut-in speed is the wind velocity at which the wind starts to have enough torque on the turbine blades to make them rotate and generate power. The rated speed is the wind velocity at which the wind turbine generates electricity at full power. The electricity production above the rated speed is generally stable until the wind speed reaches the cut-out speed. The Cut-out speed is the wind velocity at which the wind turbine is shut off to prevent damage to the rotor [30]. Wpot is therefore expressed as [7]:

$$Wpot_{h,g,a} = \begin{Bmatrix} 0 \quad if\, VO < V_{h,g,a} < VI \\ \frac{V_{h,g,a}{}^3 - VI^3}{VR^3 - VI^3} if\, VI \quad \leq V_{h,g,a} < VR \\ 1 \quad if\, V_{h,g,a} = VR \end{Bmatrix} \tag{6}$$

Where $V_{h,g,a}$ is the wind speed at turbine height (m/s), VI the cut-in speed, VR the rated speed, and VO the cut-out speed. The a is the index for the set of altitudes (80, 100, 120, 150 m).

We assumed one power curve for all onshore and offshore turbines, as there seems to be relatively little difference between the turbines. The power curve of the SIEMENS-3.0–108 was selected with a cut-in of 3.0 m/s, rated speed of 12 m/s, and a cut-out speed of 25 m/s. Wpot is calculated for every 6-h timestep on the four altitudes. To calculate the electricity production, the turbines at each altitude are multiplied with the Wpot that is closest to the hub height. The final wind production per grid cell is the sum of the production on the different altitudes.

2.4.3. Energy yield

For a more comprehensible result the daily production in MJ is converted to the energy yield in full load hours (FLH).

$$FLH_{d,r} = \frac{PO_{d,r}}{\mathrm{ICd,\ r}} / 3600 \tag{7}$$

Where FLH is the energy yield in full load hours of the installed capacity, and r is the index for the European regions.

The yield represents the amount of electricity that is produced if the capacity produces at nominal power for the given amount of hours. The advantage of using the yield is the small numbers (maximum 24 per day) that are easy to compare. A disadvantage is that the installed amount of capacity has to be known to reproduce the actual amount of produced electricity (see Table 2 for installed capacity per region).

3. Results

3.1. PVpot and Wpot in 2050 compared 1981–2010 period

Figs. 2–5 compare PVpot and Wpot under 2050 weather conditions in the four scenarios with those under average observed weather conditions in period 1981–2010.

3.1.1. Effects in summer

In the positive sNAO phase, PVpot increases moderately by 0.4–1.6% point (pp) on average in the whole of Europe compared to the observations, except for Norway and southern Iberia where it decreases. The decrease in Iberia is the result of a strong increase in temperature, caused by drier conditions, this temperature increase reduces the efficiency of solar panels.

While in the positive sNAO phase the storm track heads north from northern Scotland over the Atlantic resulting in cloudy conditions along the Norwegian coast, it heads south eastwards in the negative sNAO phase resulting in more cloudy conditions in whole northern Europe

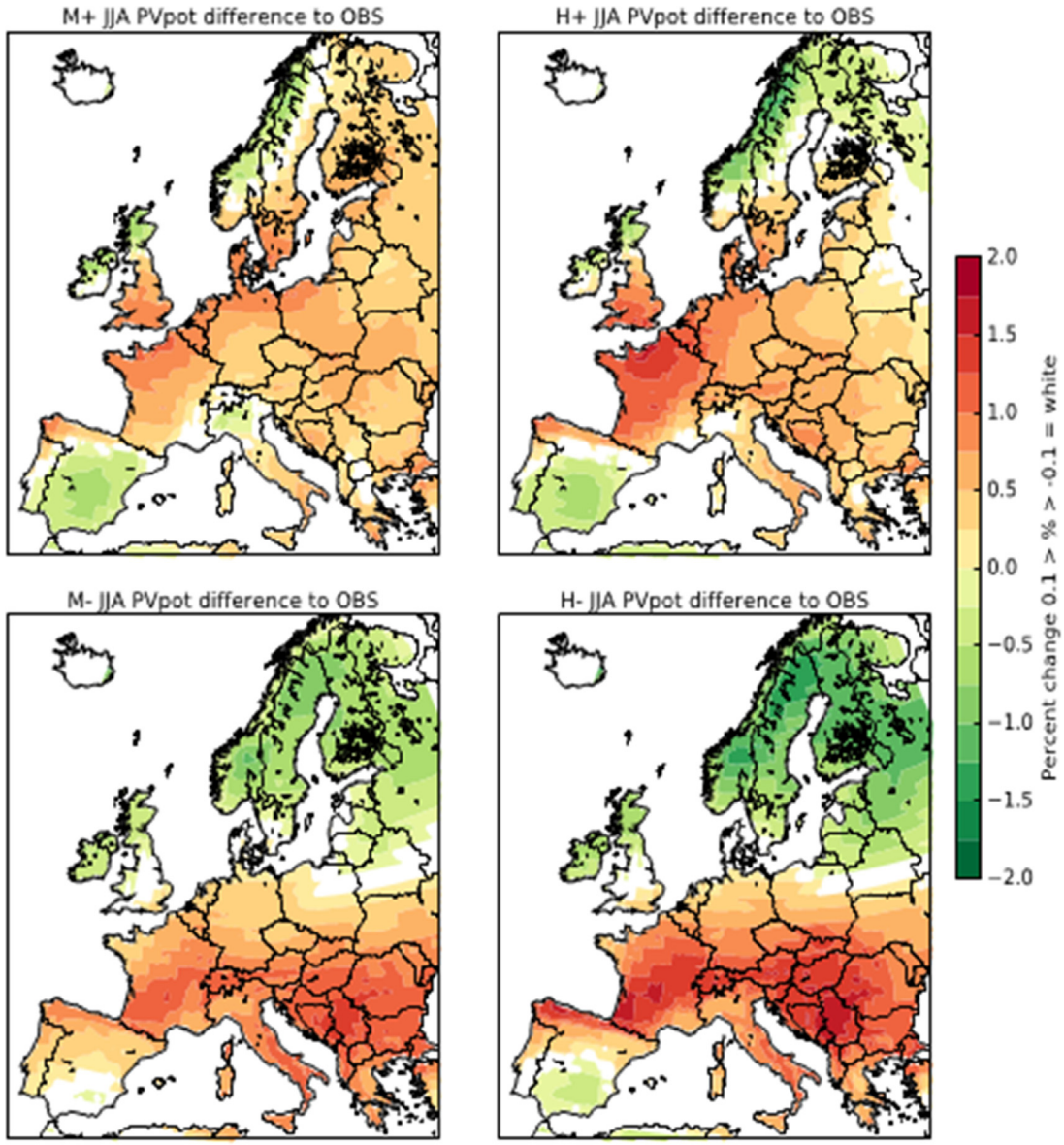

Fig. 2. Difference (in pp) between the average PVpot in the summer (JJA) under 2050 weather conditions in each scenario and those under observed weather conditions (in 1981–2010). The upper two represent the sNAO positive phase, the lower two the negative sNAO phase. The moderate and high global warming scenarios are shown on the left and right, respectively.

and consequently 0.8 – 2 pp lower PVpot. Continental Europe sees a significant increase of 1 – 2 pp in the negative sNAO phase, especially in central and southern regions.

Unlike PVpot, Wpot decreases significantly in the positive sNAO phase in Europe: by 4–8 pp from the west of southern England across the channel to the southern North Sea region, and in the rest of Europe by 2–4 pp. This relates to the position of the storm track, which brings the most windy conditions to the north-eastern Atlantic and calm conditions over most of Europe. In the negative phase of the sNAO, an increase in wind power is observed in Scotland, the North Sea, southern Scandinavia and the Baltic.

3.1.2. Effects in winter

The positive NAO phase has a limited impact on PVpot over Europe. In most of Europe it causes a low to moderate decrease: 0.2–0.4 pp in western Europe, and 0.4 – 1.6 pp in central and eastern Europe. Only along the Mediterranean coast, it results in an increase which is highest on the Iberian Peninsula (up to 2 pp). In the positive phase of the NAO, the storm track – which brings cloudy conditions - is well-developed and wide and its position is over the British Isles and southern Scandinavia.

The negative phase of the NAO leads to a strong decrease in PVpot for the whole of continental Europe, including the largest part of the Iberian peninsula, ranging from 0 to 1.6 pp. Only the coasts of Norway and Scotland see a slight increase in PVpot.

In contrast to PVpot, Wpot is strongly influenced by the positive NAO phase. In countries around the North Sea and the Baltic Sea it increases by 6–12 pp, while in southern Europe and around the Mediterranean sea it decreases by 2–8 pp. For the Wpot the negative phase of the NAO leads to a decrease ranging to 10 pp in northern regions. In the south there is an increase of 0–4 pp, however, many white spots indicating an irregular spatial pattern of change.

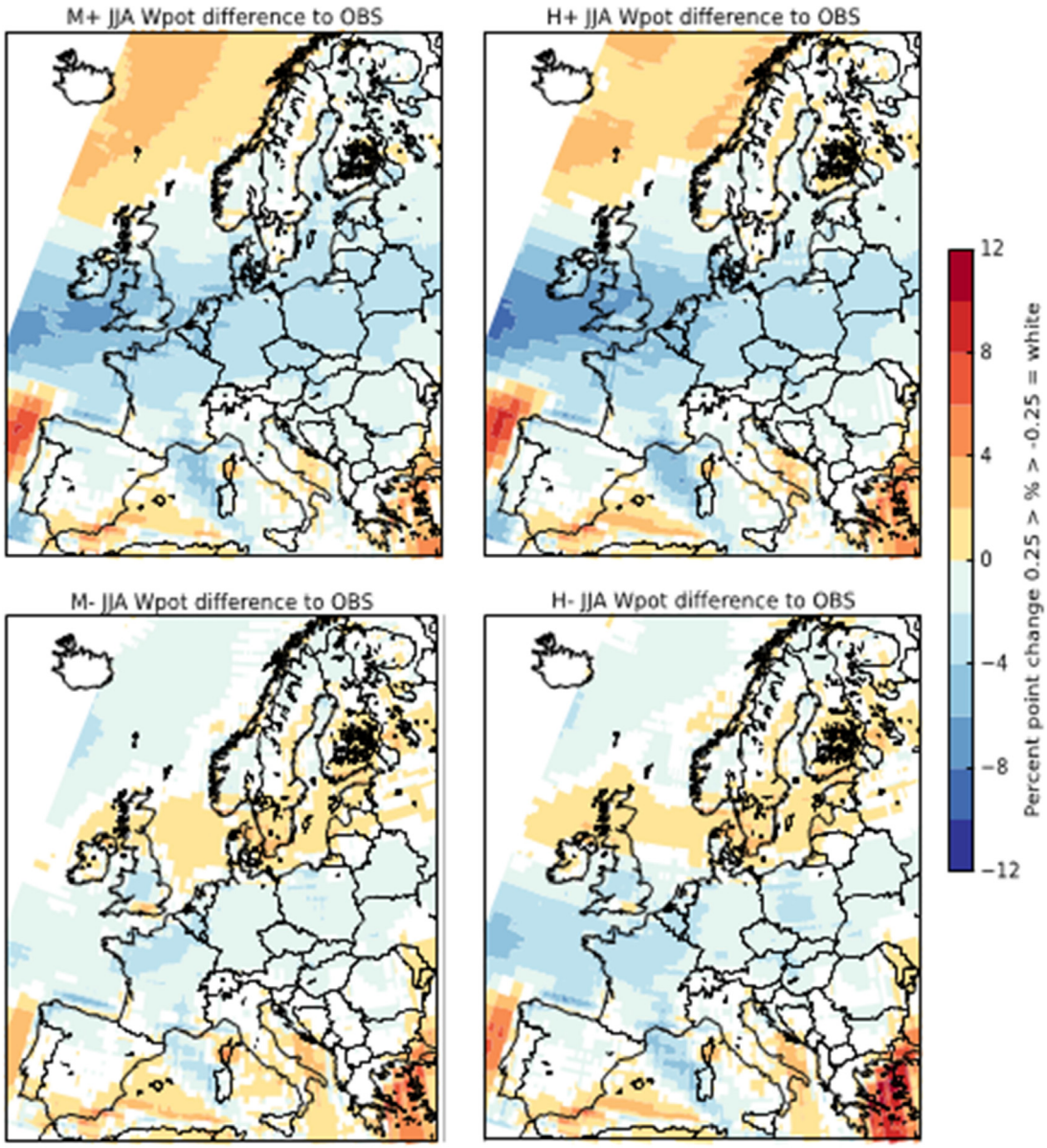

Fig. 3. Difference (in pp) the average Wpot at 80 m in the summer (JJA) under 2050 weather conditions in each scenario with those under observed weather conditions (in 1981–2010). The upper two represent the sNAO positive phase, the lower two the negative sNAO phase. The moderate and high global warming scenarios are shown on the left and right, respectively.

3.1.2.1. Impact of climate change versus NAO/sNAO phase. Overall the impact of climate change on the energy yield is low compared to the changes observed due to the opposing phases of both the NAO in winter and the sNAO in summer. Figs. 2 and 3 clearly show little difference in average PVpot and Wpot between the M and H scenarios, and clear differences between the NAO/sNAO phases. In some scenarios climate change affects the intensity of the projected output changes, but the directions of change are determined by the NAO/sNAO phases. Both for Wpot and PVpot, we observed that the changes in energy yield are much larger between the two phases of the NAO/sNAO than between the moderate and warm scenarios.

3.2. Impact of climate change and NAO/sNAO on energy yield and variability

3.2.1. Impacts on energy yield

Table 3 presents the average total European production as a function of the sNAO/NAO phases for both I-RES sources. In the summer PV is by far the largest source of electricity, producing more than two thirds of the total I-RES output aggregated over Europe. The total yield averaged over the summers with a negative sNAO phase is 3.8 higher than those with a positive sNAO phase, with a 0.6% and 10.3% increase from PV and wind, respectively

During winter the wind power is by far the largest contributing source, responsible for approximately three quarters of the European I-RES output. In the winter the positive NAO phase leads to a 10.8% higher production than in the negative phase with the PV yield increasing with 2.6% and the wind yield with 13.4%.

Fig. 6 presents the climate change impact based on the H scenarios compared to the observed weather period 1981–2010 and the impact of the NAO/sNAO phases per region. The impact of climate change indicates a change over a long time period, where the impact of NAO/sNAO indicates a change that is variable on a monthly to seasonal time scale. The figure shows that climate change will affect the potential

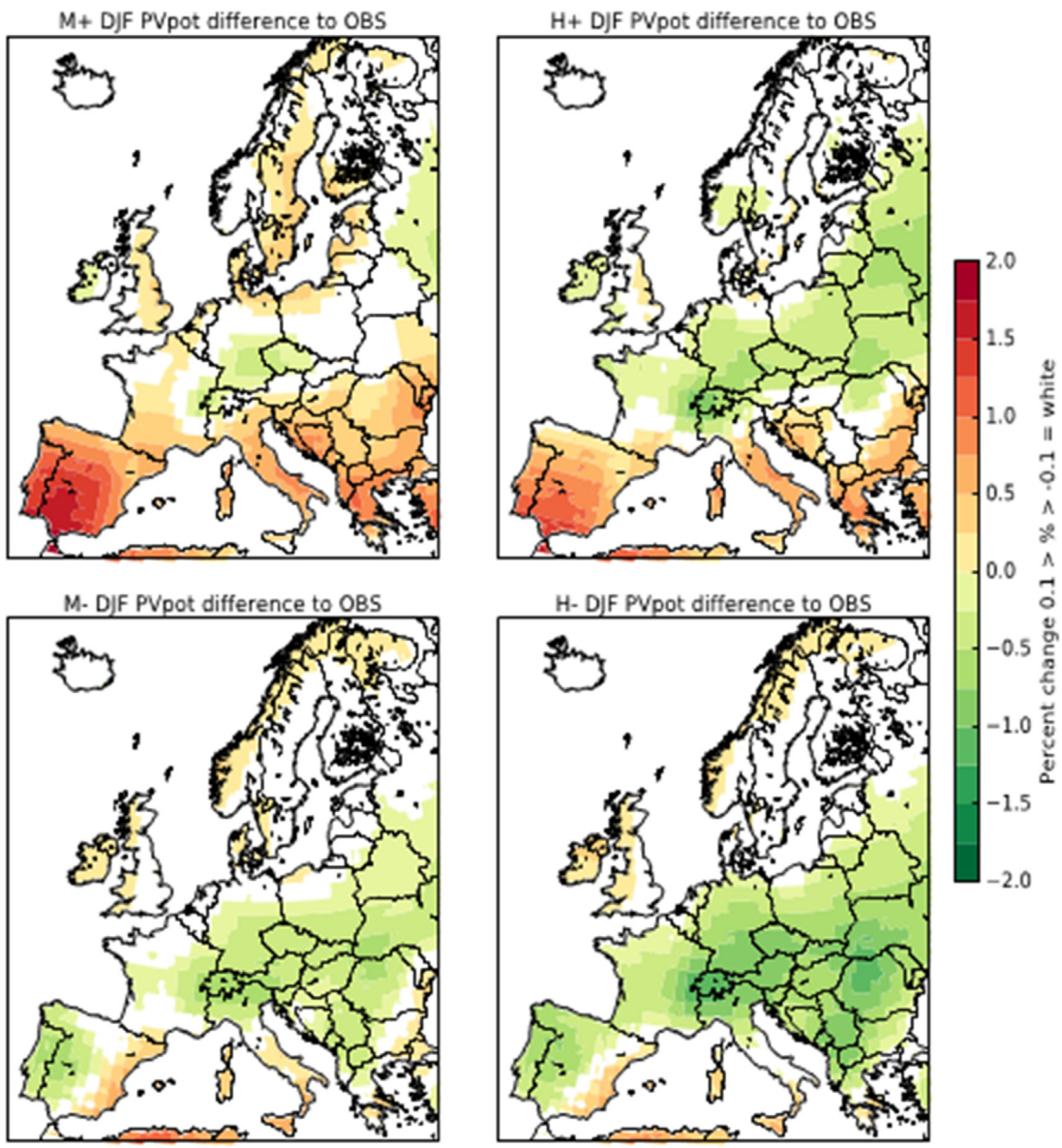

Fig. 4. Difference (in pp) between the average PVpot in the winter (DJF) under 2050 weather conditions in each scenario and those under observed weather conditions (in 1981–2010). The upper two represent the sNAO positive phase, the lower two the negative sNAO phase. The moderate and high global warming scenarios are shown on the left and right, respectively.

yields of wind and PV in all regions compared to potential yield under observed weather conditions.

On average wind output will decrease in the H scenarios. However, the climate change impact is lower in most regions compared to the impact of the NAO phases on the wind output. Only exceptions are central Europe, France, and Iberia in the summer season, and central Europe in the winter season. Especially central Europe will have to cope with lower wind output in all H scenarios.

The impact of climate change on the PV output is limited (not more than 4% compared to average OBS data) and causes a slight increase in the summer and small decrease in the winter. In this case, the climate change signal has a slightly stronger impact than the sNAO/NAO phases. The results agree with previous findings of Wild et al. [6] who estimate a 0.5–1% increase per decade in PV output under the RCP 8.5 scenario in Europe with the exception of northern states. Also our results show the same spatial pattern due to climate change as Jerez et al. [8] find for the south of Europe. However, their decrease in the north of Europe is significantly higher.

3.2.2. Impacts on variability

As shown in Fig. 6, median wind yield increases in mid-latitude regions like Benelux-Germany in the winter during the +NAO phase, while it increases in a Mediterranean region like the Iberian Peninsula during the -NAO phase. For these two different regions, the probability density functions of the daily yields are presented in Fig. 7 in order to assess whether climate change or the NAO/sNAO phases also influence the variability in these day-to-day yields. The box plots show a strong impact of the NAO but hardly any impact of climate change on winter wind yields. The phase of the NAO does not have a large impact on the variability as can be seen by the same size of the box plots in all

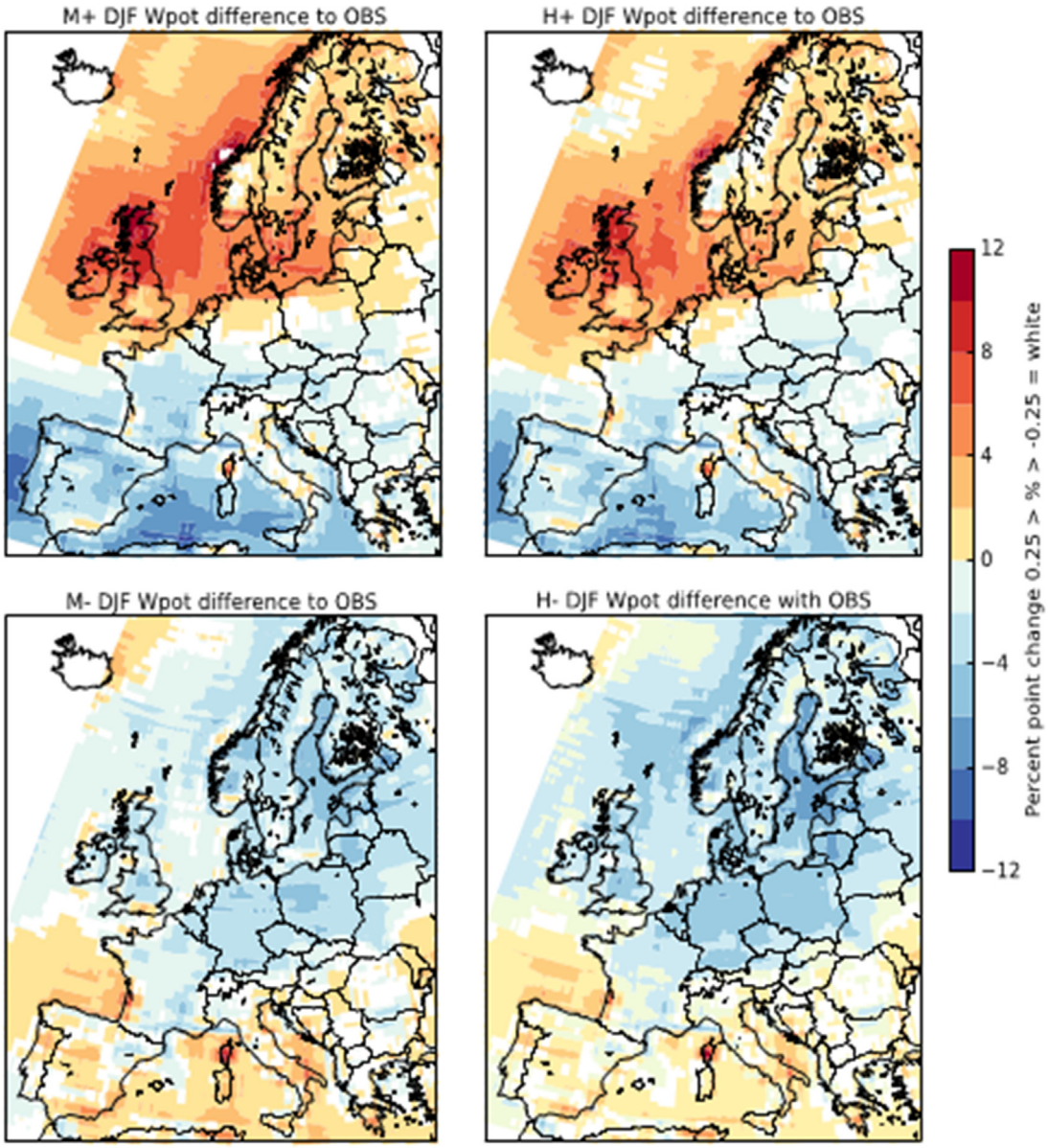

Fig. 5. Difference (in pp) the average Wpot at 80 m in the winter (DJF) under 2050 weather conditions in each scenario with those under observed weather conditions (in 1981–2010). The upper two represent the sNAO positive phase, the lower two the negative sNAO phase. The moderate and high global warming scenarios are shown on the left and right, respectively.

Table 3
Average total European production from I-RES sources in the H scenarios.

		Total production (TW h)	PV production (TW h)	Wind Production (TW h)
Summer	H+	603	415	188
	H-	626	418	208
Winter	H+	534	119	415
	H-	482	116	366

scenarios, which only shift up or down according to the phases. The CoV (defined as the standard deviation divided by the mean) of Benelux-Germany increases from 0.51 in the positive phase to 0.58 in the negative phase, while it decreases in the Iberian Peninsula from 1.05 to 0.94. For all regions a small but clear link between a higher CoV and the lower yield phase is observed. Note that the 5th percentiles of the daily wind yields vary with the NAO phase much less than the 25th percentiles. For the daily yields, this indicates that the phase of NAO affects the mean and quartiles more than the tails of the distribution.

In order to look into the variability multi-day periods of wind power yield, the 5th percentiles of the 3, 5, 11 day running mean are shown in Fig. 7. Similar to the 5th percentiles of the 1-day wind yield, these percentiles show lower values for the negative NAO phases in Benelux-Germany, with the difference in the percentiles between positive and negative phase amplifying when longer windows are considered. This indicates an increasing impact of the NAO on the tails of the wind yield distribution when longer aggregation periods are considered.

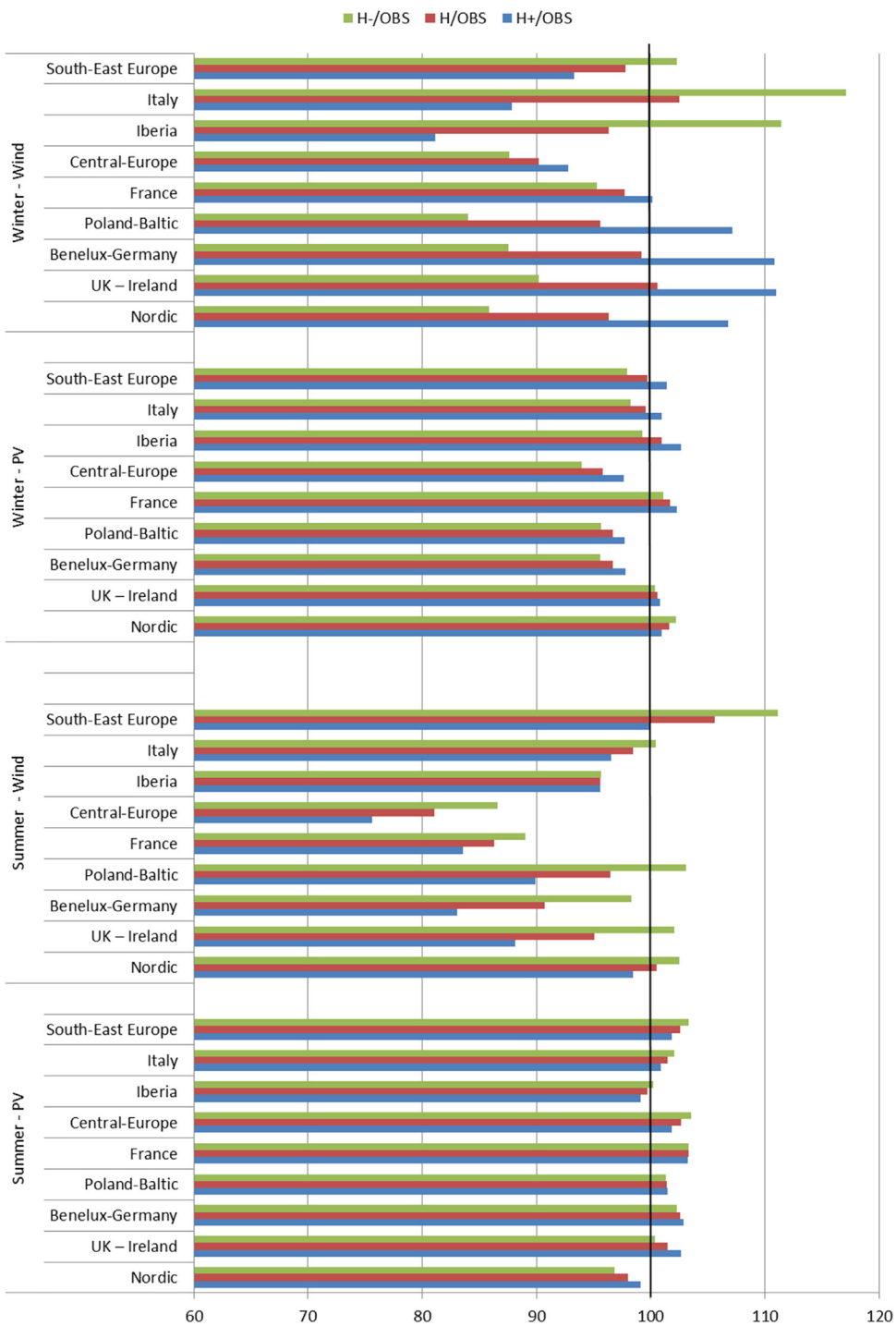

Fig. 6. Median daily I-RES yields of average H climate scenario and sNAO/NAO phases compared to the OBS data set (OBS yield is set to 100). Results for winter and summer are depicted on the top and bottom, respectively.

3.3. Identification of winters with very low energy yields

To analyse the impact of the NAO phase on the security of renewable energy supply, winter months with extremely low renewable energy yield are identified. The three winters in the climate simulations with the lowest absolute yield of around 75 TW h instead of the average 116 TW h in the Benelux-Germany (see Table 4) are all characterised by a negative NAO. The yields in these winters are 34%, 37%, and 36% lower than the average for sample 003, 080, and 101 respectively. The difference for single months is significantly larger: December of sample 003 is the lowest producing month of these winters, with a wind yield that is 66% lower than the long-term December average.

The maps in Fig. 8 shows the relative change in Wpot and PVpot of the months with the lowest I-RES yield in these three winters compared

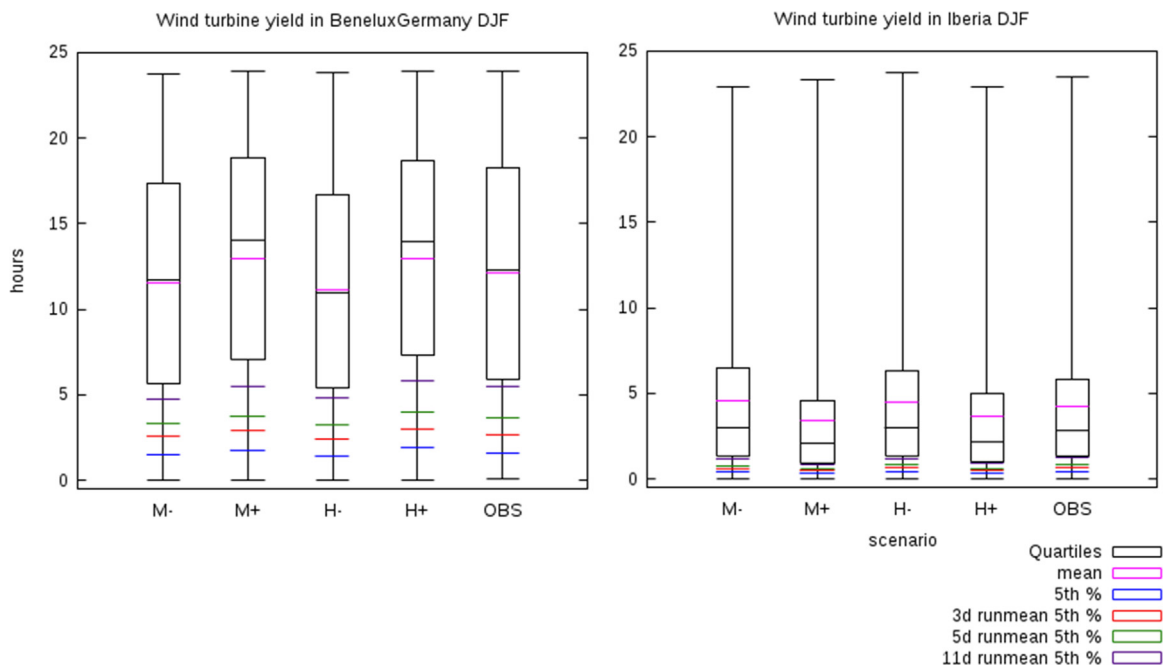

Fig. 7. Box plots of daily wind yields (FLH) in the winter for the Benelux-Germany and Iberian Peninsula regions. The box plots indicate the 25th, the median and 75th percentiles in wind turbine yields.

Table 4
Absolute power yield for Benelux-Germany for each I-RES source and total I-RES on average in the H scenarios and for the three lowest production samples.

	Winter (DJF)			Lowest yield months	
in TW h	PV & wind	PV	Wind	Wind – DEC	Wind – FEB
Average over H+ and H- scenarios	116	11	105	35	31
Sample 003	75	12	63	12	
Sample 080	73	12	61		12
Sample 101	74	10	64	17	

to the average of the H scenarios. In these months the Wpot decreases significantly in nearly all of Europe, in some regions with more than 75% of their average potential. In one of the minimum yield months (model year 101), very low Wpot is combined with lower PVpot due to a stagnant high-pressure area over Europe which brings the dull weather with calm and cloudy conditions. The other two months show classic negative phase patterns: Wpot decreases and the PVpot increases as dry eastern winds result in less cloud cover and therefore an increase in the PVpot. However, this increase is negligible compared to the loss of wind power yield due to the low irradiation in the winter.

Fig. 8 also shows the Heating Degree Days (HDD) (based on 18 °C reference temperature) which represent the demand for energy used for heating [31,32]. With a need to switch away from conventional fuels and save energy, heat pumps will likely supply a large proportion of the future domestic heat demand resulting in a higher electricity demand. The frigid continental winds carry cold air from the north and east to Europe cause a very strong increase in the amount of HDDs, up to 30% more for western Europe and in sample 080 even up to 50% for South-East Europe. Apparently, a reduction of up to 75% in the electricity supply from wind turbines in high wind-dependent regions can coincide with a strong increase in energy demand.

Based on the EC-Earth climate model it is estimated that these 'worst-case' winters, based on taking the numbers of samples observed (3) divided by the number of winters in the M or H scenarios (~240) can occur once every 80 years. However, single months with a very low production are likely to occur much more often.

4. Conclusion

This study assessed the impact of climate change and climate variability on both PV and wind power output. We found that although climate change is likely to have significant impact on future PV and wind power output in Europe, its effects, especially for wind power, are outweighed by the strong and highly variable impact of the NAO/sNAO. Variability in the large-scale atmospheric circulation is able to induce average median yield differences of 20–30% for high wind potential regions. Due to the NAO variability also periods were identified with persistent calm conditions over Europe linked to the inflow of frigid arctic air resulting in a decrease in wind power accompanied with extreme cold which increases the heating degree days with 30%. The results of the study imply that if requirements for the power system including back up capacity take into account the weather variability, the power system can also cope with the climate change impacts.

A sensitivity analysis showed that most simplifications made in this study (i.e. a constant temperature and irradiation during the day and an average day length for the whole of Europe, the same wind turbine height), only affected the absolute results and not the relative differences between scenarios. However, further research should provide more insights into the impact of different power curves for wind turbines on the relative differences. In this study the NAO/sNAO were assumed to be phenomena independent of climate change. Projected trends in NAO indices are generally found to have small amplitude and often insignificant compared to natural internal

variations [29–31]. In agreement with this a recent study showed that the changes in NAO are insignificant for EC-Earth [32]. This was confirmed for the simulations used in this study (not shown). Further research could focus on a deeper understanding of the NAO itself. As the largest uncertainty stems from the model data, the results of this research could be refined by a similar approach based on multiple climate simulation models or observational data.

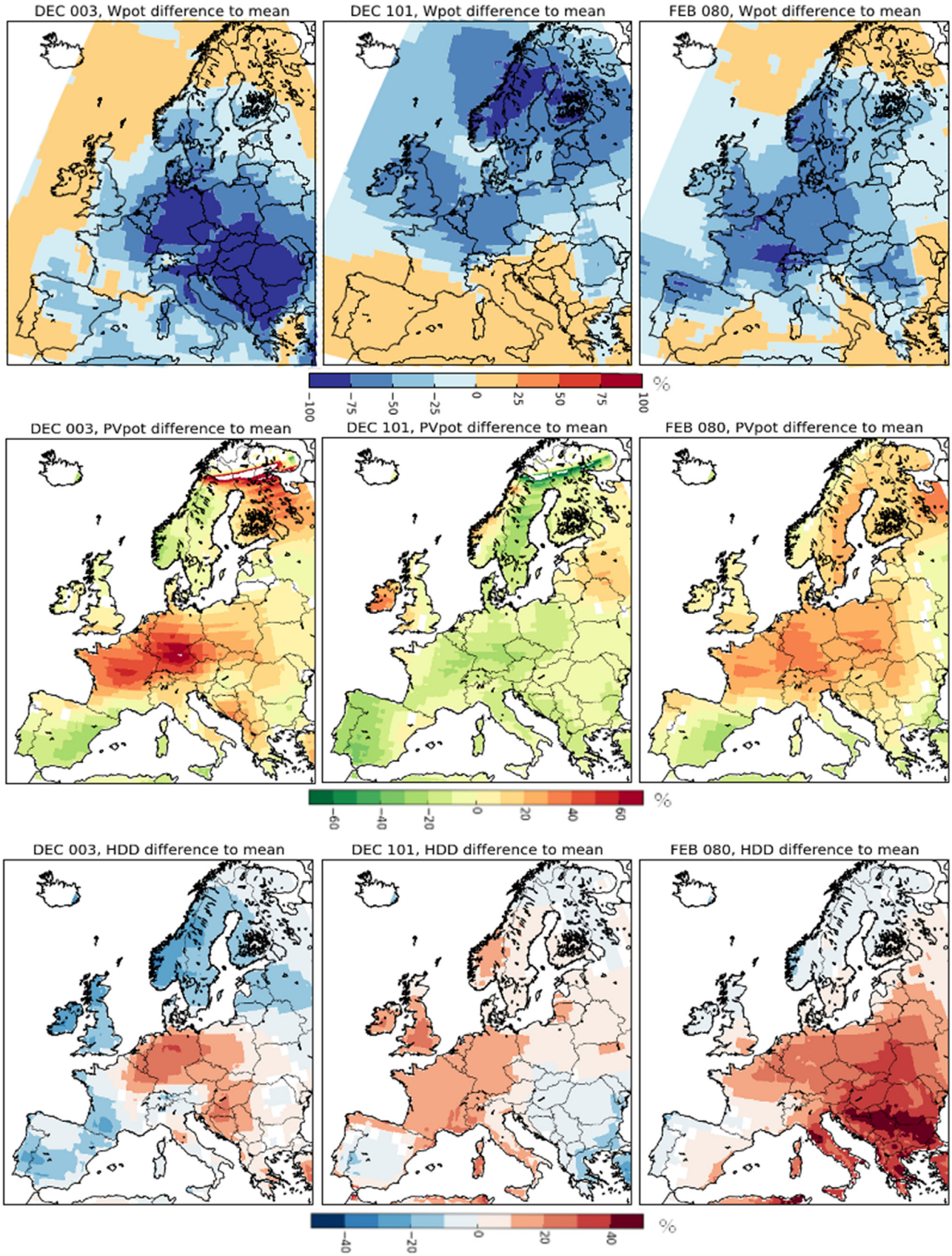

Fig. 8. Presenting the Wpot, PVpot, and HDD percentage differences between the three lowest production months in winter and the average of the respective months over both NAO phases.

Acknowledgement

We thank all reviewers for their valuable comments on an earlier version of this paper.

Appendix A. -Bias Correction

All climate models suffer from biases in their output. These biases result in e.g. surface temperatures which are somewhat cooler or warmer than observations, under- or overestimations of wind speed and estimates of cloud cover which poorly compare to observations. In general, there are two distinct approaches to alleviate these issues. Both approaches are used to adjust the model output in this study.

Bias correction

There are numerous methods to correct biases in model outputs. The most complex methods, which can only be applied to regional climate models, is to involve the atmospheric circulation and adjust model output using information from observations and the actual simulated weather. In this study a less advanced approach is used by adjusting the mean modelled climate with observed climatological fields. The difference between the mean observed climate and the mean modelled climate (which is the mean bias of the model) is added to the model output. This approach is applied to each modelled parameter (like temperature, radiation and wind speed). In this approach, care is taken not to produce negative wind speeds (which would be possible if the modelled wind speeds are overestimated compared to observations) or radiation values which are negative or exceed the maximally possible values. In general, this bias correction simply adjusts the modelled output in the direction of the observed values, making sure that at least the means coincide. Note that this adjustment does not affect the variability of the model. If a bias in the CoV is observed, this bias will not disappear with this approach.

Comparison against model climatology

Although the mean climate in global climate models suffers from biases, this does not mean that the *change* in climate is modelled unrealistically. A comparison between various global climate models indicates that the level of agreement in climate change in a benchmark test situation, is far more uniform between the models than the actual mean climate simulated by these models. This notion is central in many climate central studies, where changes are presented as deviations from the model climatology. This approach is used in this study as well.

References

[1] Edenhofer O, Pichs-Madruga R, Sokona Y, Seyboth K, Eickemeier P, Matschoss P. et al. IPCC: Summary for Policymakers. In: IPCC Special Report on Renewable Energy Sources and Climate Change Mitigation. Geneva: 2011. 〈http://dx.doi.org/10.5860/CHOICE.49-6309〉; 2011.
[2] Pryor SC, Barthelmie RJ. Climate change impacts on wind energy: a review. Renew Sustain Energy Rev 2010;14:430–7. https://doi.org/10.1016/j.rser.2009.07.028.
[3] European Commission. European commission on climate conference Paris. 2016. 〈http://ec.europa.eu/clima/policies/international/negotiations/paris/ixndex_en.htm〉 [accessed 9 March 2016].
[4] Hueging H, Haas R, Born K, Jacob D, Pinto JG. Regional changes in wind energy potential over Europe using regional climate model ensemble projections. J Appl Meteorol Climatol 2013;52:903–17. https://doi.org/10.1175/JAMC-D-12-086.1.
[5] Reyers M, Pinto JG, Moemken J. Statistical-dynamical downscaling for wind energy potentials: evaluation and applications to decadal hindcasts and climate change projections. Int J Climatol 2015;35:229–44. https://doi.org/10.1002/joc.3975.
[6] Wild M, Folini D, Henschel F, Fischer N, Müller B. Projections of long-term changes in solar radiation based on CMIP5 climate models and their influence on energy yields of photovoltaic systems. Sol Energy 2015;116:12–24. https://doi.org/10.1016/j.solener.2015.03.039.
[7] Jerez S, Thais F, Tobin I, Wild M, Colette A, Yiou P, et al. The CLIMIX model: a tool to create and evaluate spatially-resolved scenarios of photovoltaic and wind power development. Renew Sustain Energy Rev 2015;42:1–15. https://doi.org/10.1016/j.rser.2014.09.041.
[8] Jerez S, Tobin I, Vautard R, Montávez JP, López-Romero JM, Thais F, et al. The impact of climate change on photovoltaic power generation in Europe. Nat Commun 2015;6:10014. https://doi.org/10.1038/ncomms10014.
[9] Tobin I, Vautard R, Balog I, Bron FM, Jerez S, Ruti PM, et al. Assessing climate change impacts on European wind energy from ENSEMBLES high-resolution climate projections. Clim Change 2015;128:99–112. https://doi.org/10.1007/s10584-014-1291-0.
[10] Tobin I, Jerez S, Vautard R, Thais F, van Meijgaard E, Prein A, et al. Climate change impacts on the power generation potential of a European mid-century wind farms scenario. Environ Res Lett 2016;11:34013. https://doi.org/10.1088/1748-9326/11/3/034013.
[11] Greatbatch R. Stochastic Environmental Research and Risk Assessment; 14: 213. 〈https://doi.org/10.1007/s004770000047〉; 2000.
[12] Hurrell JW. Decadal trends in the North Atlantic oscillation: regional temperatures and precipitation. Science 1995;269:676–9. https://doi.org/10.1126/science.269.5224.676.
[13] Folland CK, Knight J, Linderholm HW, Fereday D, Ineson S, Hurrel JW. The summer North Atlantic oscillation: past, present, and future. J Clim 2009;22:1082–103. https://doi.org/10.1175/2008JCLI2459.1.
[14] van den Besselaar EJM, Klein Tank AMG, van der Schrier G. Influence of circulation types on temperature extremes in Europe. Theor Appl Climatol 2010;99:431–9. https://doi.org/10.1007/s00704-009-0153-6.
[15] Brayshaw DJ, Troccoli A, Fordham R, Methven J. The impact of large scale atmospheric circulation patterns on wind power generation and its potential predictability: a case study over the UK. Renew Energy 2011;36:2087–96. https://doi.org/10.1016/j.renew.2011.01.025.
[16] Jerez S, Trigo RM, Vicente-Serrano SM, Pozo-VáZquez D, Lorente-Plazas R, Lorenzo-Lacruz J, et al. The impact of the North Atlantic Oscillation on renewable energy resources in Southwestern Europe. J Appl Meteorol Climatol 2013;52:2204–25. https://doi.org/10.1175/JAMC-D-12-0257.1.
[17] Pozo-Vázquez D, Tovar-Pescador J. NAO and solar radiation variability in the European North Atlantic region. Geophys Res Lett 2004;31:4. https://doi.org/10.1029/2003GL018502.
[18] Pozo-Vázquez D, Santos-Alamillos F, Lara-Fanego V, Ruiz-Arias J, Tovar- Pescador J. 2011: The Impact of the NAO on the Solar and Wind Energy Resources in the Mediterranean Area. Hydrological, Socioeconomic and Ecological Impacts of the North Atlantic Oscillation in the Mediterranean Region. Vicente-Serrano, Sergio. and Trigo, Ricardo. Springer, 18 pp.
[19] Hazeleger W, Wang X, Severijns C, Stefuanescu S, Bintanja R, Sterl A, et al. EC-Earth V2. 2: description and validation of a new seamless earth system prediction model. Clim Dyn 2012;39:2611–29. https://doi.org/10.1007/s00382-011-1228-5.
[20] KNMI. KNMI'14 climate scenario's for the Netherlands; A guide for professionals in climate adaptation. The Netherlands: KNMI, De Bilt; 2014. p. 34.
[21] Haylock MR, Hofstra N, Klein Tank AMG, Klok EJ, Jones PD, New M. European daily higher-solution gridded data set of surface temperature and precipitation for 1950–2006. J Geophys Res (Atmospheres) 2008;113:D20119. https://doi.org/10.1029/2008JD010201.
[22] Dahlgren P, Gustafsson N. Assimilating host model information into a limited area model. Tellus Ser A Dyn Meteorol Oceanogr 2012:64. https://doi.org/10.3402/tellusa.v64i0.15836.
[23] Dee DP, et al. The era-Interim reanalysis: configuration and performance of the data assimilation system. Q J R Meteorol Soc 2010;137:553–97. https://doi.org/10.1002/qj.
[24] ECF. Roadmap 2050 a practival guide to a prosperous, low-carbon Europe; 2010.
[25] Schlachtberger DP, Brown Tom, Schramm A, Greiner Martin. The benefits of cooperation in a highly renewable European electricity network. Energy 2017;134:469–81. [06.06.2017].
[26] Mavromatakis F, Makrides G, Georghiou G, Pothrakis A, Franghiadakis Y, Drakakis E, et al. Modeling the photovoltaic potential of a site. Renew Energy 2010;35:1387–90. https://doi.org/10.1016/j.renene.2009.11.010.
[27] Sark WGJHM van, N.H. Reich BM. Review of PV Performance Ratio Development. World Renew Energy Forum Congr XII 2012:1–6. 〈http://dx.doi.org/10.13140/2.1.2138.7204〉.
[28] Chenni R, Makhlouf M, Kerbache T, Bouzid A. A detailed modeling method for photovoltaic cells. Energy 2007;32:1724–30. https://doi.org/10.1016/j.energy.2006.12.006.
[29] Twidell J, Weir T. Renewable Energy Resources. 3rd ed New York: Routledge; 2006. https://doi.org/10.4324/9780203478721.
[30] The wind program n.d. 〈http://www.wind-power-program.com〉 [accessed 5 April 2016].
[31] Isaac M, van Vuuren DP. Modeling global residential sector energy demand for heating and air conditioning in the context of climate change. Energy Policy 2009;37:507–21. https://doi.org/10.1016/j.enpol.2008.09.051.
[32] Blok K. Introduction to energy analysis. Amsterdam: Techne Press; 2006.